Vibrational dynamics of hydrogen in proteins

Derya Vural and Henry R. Glyde
Department of Physics and Astronomy, University of Delaware, Newark, Delaware 19716-2570, USA
(Received 24 January 2010; revised manuscript received 1 November 2010; published 31 March 2011)

Biological macromolecules expand with increasing temperature and this dynamic expansion is associated with the onset of function. The expansion is typically characterized by the mean square vibrational displacement (MSD), $\langle u^2\rangle$, of specific constituents such as hydrogen within the macromolecules. The $\langle u^2\rangle$ increases with increasing temperature and the slope of $\langle u^2\rangle$ versus temperature can increase significantly at a temperature T_D identified as a dynamical transition. We illustrate that the observed expansion and change in slope of $\langle u^2\rangle$ with temperature at T_D can be reproduced within a simple model of the vibration, an atom in an anharmonic potential, $V(u)$. Given $V(u)$, only the temperature is varied in the model. A simple Gaussian potential or a potential containing a hard wall is particularly effective is reproducing the observed change in the slope of $\langle u^2\rangle$ with temperature around T_D.

DOI: 10.1103/PhysRevE.83.031922 PACS number(s): 87.14.E−, 61.05.fg

I. INTRODUCTION

Many biological macromolecules undergo a dynamical transition [1–10] or crossover at a temperature $T_D \sim$ 200–230 K. The crossover can be characterized by a significant increase in the slope of the mean square displacement (MSD), $\langle u^2\rangle$, of atoms in the molecule with temperature at T_D. Above T_D, the $\langle u^2\rangle$ is large, the macromolecule is more flexible and atoms in the macromolecule traverse larger distances and sample new environments. This dynamical crossover is associated with the onset of function or activity in the macromolecule.

In the classical limit and in a harmonic approximation [4,9], the MSD arising from vibration is $\langle u^2\rangle = k_B T/\phi$ where k_B is the Boltzmann constant, T is the temperature and ϕ is a harmonic force constant. An increase in slope of $\langle u^2\rangle$ vs. T at $T \simeq T_D$ suggests a reduction in the effective force constant ϕ at $T \simeq T_D$. Often the slope begins to increase somewhat at lower temperatures ($T \simeq 100$ K) and the changes with temperature are continuous [5]. However, there usually remains a marked change in slope at T_D. The magnitude of the change in slope depends on the degree of hydration of the protein [2,4–6] and many other factors. The observed change in slope can be reproduced in molecular dynamics simulations of proteins [1,8].

The change in slope is observed in hydrated proteins, in DNA and in RNA. Typical examples are hydrated lyzozyme [3], myoglobin [9], and purple membrane bacteriorhodopsin [2,5]. The $\langle u^2\rangle$ is determined in neutron scattering [4,9,10], x-ray and Mossbauer spectroscopy [10,11], and in dielectric spectroscopy [5]. In neutron scattering, the $\langle u^2\rangle$ of hydrogen is predominantly observed, usually hydrogen bound in molecules (e.g., methyl groups). In Mossbauer spectroscopy the $\langle u^2\rangle$ of ^{57}Fe is observed. The sudden change in slope of $\langle u^2\rangle$ at T_D has been attributed to a change in the "effective elasticity" of the protein [7], to a "glass" transition in the protein [9,12,13], to the onset of thermally activated transitions and diffusion that modify the trapping cages [9,14] and to a fragile-strong crossover in the hydration water surrounding the macromolecule [15].

Our goal is simply to illustrate that a marked change in the slope of $\langle u^2\rangle$ with T can arise in the vibrational dynamics of a particle of mass M in an anharmonic potential well. This can arise, for example, in a Gaussian potential well, in which the curvature (effective force constant) decreases with increasing distance of the particle from the minimum of the well. This average distance increases with increasing $\langle u^2\rangle$. In the Gaussian well example, the increase in slope with T is gradual. However, if the potential has hard wall and soft wall components in it, an abrupt change in slope of $\langle u^2\rangle$ with T can be obtained. We consider a single particle in a 1D well and use the self-consistent harmonic (SCH) theory [16–19] to describe the dynamics of the particle in the well. The essential feature of the SCH model is that the optimum harmonic force constant ϕ is obtained as the second derivative of the potential averaged over the vibrational distribution of the particle in the well. As the $\langle u^2\rangle$ increases, a wider region of the well is sampled and the force constant, ϕ, can change (e.g., decrease) with increasing $\langle u^2\rangle$. This decrease leads to an increase in slope of $\langle u^2\rangle$ with temperature at T_D as is observed.

II. DYNAMICAL MODEL

To describe the dynamics of a particle in a potential $V(u)$ we employ the self-consistent harmonic (SCH) theory of dynamics [16–19]. In the SCH theory the aim is to determine the harmonic force constant ϕ that best describes the anharmonic dynamics. The harmonic model can be introduced via a trial harmonic Hamiltonian H_h and its corresponding density matrix ρ_h. The optimum ϕ in H_h can be determined by minimizing the Helmholtz free energy. The result is that the usual harmonic force constant $\phi(u) = (d^2V/du^2)_{u=0}$, the second derivative evaluated at the minimum of the well ($u = 0$), is replaced by

$$\phi = \int du\rho(u)\frac{d^2V(u)}{du^2}, \tag{1}$$

the second derivative averaged over the vibrational distribution $\rho(u)$ in the well. The distribution is

$$\rho(u) = [2\pi\langle u^2\rangle]^{-1/2}e^{-u^2/2\langle u^2\rangle}, \tag{2}$$

a Gaussian since we are assuming a harmonic model. The mean square displacement $\langle u^2 \rangle$ is given by the usual harmonic expression,

$$\langle u^2 \rangle = \frac{\hbar}{2M\omega} \coth\left(\frac{k_B T}{\hbar\omega}\right), \tag{3}$$

where M is the particle mass, $\omega^2 = \phi/M$ is the harmonic frequency, and $\hbar$ is Planck's constant divided by 2π. In the classical limit, $T \geqslant \theta_E = \hbar\omega/k_B$, Eq. (3) reduces to

$$\langle u^2 \rangle = \frac{k_B T}{\phi}. \tag{4}$$

Equations (1) to (3) constitute the SCH theory. It is implemented by iterating Eqs. (1), (2), and (3) until consistent beginning, for example, with an estimated value of $\langle u^2 \rangle$. The SCH can be derived by summing a class of anharmonic terms as well as by minimizing the free energy or ground state energy at $T = 0$ K.

III. RESULTS

A. Harmonic potentials

Our model of an atom in a macromolecule is a single particle in a 1D potential well. We begin with a harmonic well to introduce the model and consider low temperature to determine a low-temperature model force constant, ϕ_L, and to set the length scales. The harmonic potential is $V(u) = (1/2)\phi_L u^2$, $d^2V/du^2 = \phi_L$, the oscillator (SHO) frequency is $\omega^2 = \omega_L^2 = \phi_L/M$ and in the classical limit the $\langle u^2 \rangle$ is Eq. (4) with $\phi = \phi_L$. We choose a mass $M = 20$ Amu which is intended to represent hydrogen bonded in a molecule.

At low temperature, $T \lesssim 120$ K, the observed $\langle u^2 \rangle$ versus T in biological macromolecules is well described by a straight line, as in Eq. (4). We choose the low-temperature force constant in our model, so that $\langle u^2 \rangle = k_B T/\phi_L$ reproduces the observed straight line $\langle u^2 \rangle_{\rm obs}$ vs. T at low T. We select, arbitrarily, myoglobin hydrated with 0.38 g of D_2 O per g of protein as observed by Doster *et al.* [9]. To fix ϕ_L we introduce a convenient temperature T_0, arbitrarily choosing $T_0 = 240$ K, and extrapolate the observed myoglobin low temperature $\langle u^2 \rangle$ to T_0 and determine the length $u_0^2 \equiv \langle u^2 \rangle_{\rm obs} = k_B T_0/\phi_L$. This extrapolation of the low-temperature myoglobin $\langle u^2 \rangle$ data is shown as a solid line in Fig. 1 giving $u_0^2 = 0.1$ Å^2 at $T_0 = 240$ K. Clearly, the low temperature force constant is $(\phi_L/k_B) = T_0/u_0^2$. We also use u_0 and T_0 as convenient length and temperature scales, respectively.

We use (ϕ_L/k_B) as the low-temperature force constant in all potentials. When the potential well $V(u)$ is not harmonic, we adjust the parameters in $V(u)$ (in units of k_B) so that the low-temperature force constant is $(d^2V/du^2)_{u=0} = (\phi_L/k_B) = T_0/u_0^2$. In this way all potentials have the same initial slope of $\langle u^2 \rangle$ vs. T at low temperature and they differ only in their higher temperature behavior ($T \gtrsim T_0/2$).

The inset of Fig. 1(a) shows the harmonic potential $V(u) = (1/2)\phi_L u^2$ in the dimensionless length $x = u/u_0$ in the form $\upsilon(x) = V(x)/k_B T_0$. Using $\phi_L/k_B = T_0/u_0^2$, $\upsilon(x) = (1/2)x^2$. Figure 1(b) shows the harmonic potential and vibrational distribution $\rho(x) = [2\pi\langle x^2 \rangle]^{-1/2} \exp[-x^2/2\langle x^2 \rangle]$ at three temperatures where $\langle x^2 \rangle = \langle u^2 \rangle/u_0^2$. Since $d^2\upsilon(x)/dx^2 = 1$ for all x for the harmonic potential, the SCH force constant ϕ given by Eq. (1) remains $\phi = \phi_L$ at all T independent of the width of $\rho(x)$. For a harmonic potential, the SCH model is the same as the harmonic approximation.

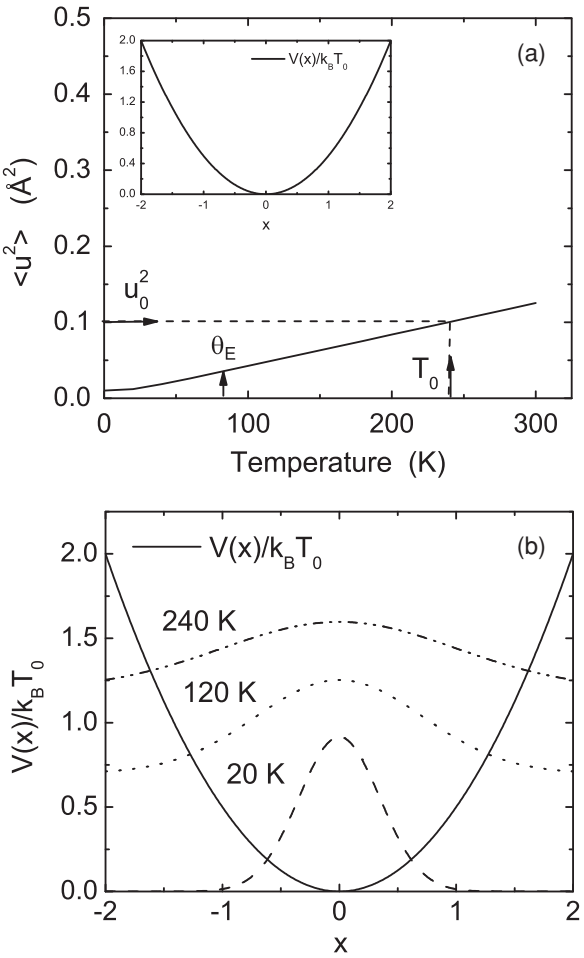

FIG. 1. (a) The mean square vibrational displacement, (MSD), $\langle u^2 \rangle$, given by Eq. (3) of an atom in a harmonic well. The slope of $\langle u^2 \rangle$ vs. T in the classical limit, $T \geqslant \theta_E$, is given by $\langle u^2 \rangle = k_B T/\phi_L$. We choose the low temperature force constant ϕ_L in our model so that it reproduces the observed slope of myoglobin at low temperature, i.e., $u_0^2 = \langle u^2 \rangle_{\rm obs} = k_B T_0/\phi_L$ where $u_0^2 = 0.1$ Å^2 is the observed MSD at temperature T_0. (b) The vibrational distribution $\rho(x)$ in harmonic well $\upsilon(x) = V(u)/k_B T_0$, $x = u/u_0$ at three temperatures.

B. Symmetric potentials

Figure 2(a) shows the $\langle u^2 \rangle$ predicted by the SCH theory for a particle in a Gaussian potential,

$$V(u) = -Ae^{-\alpha u^2}, \tag{5}$$

where A and α are adjustable parameters. In this case d^2V/du^2 decreases with increasing u and the SCH force constant ϕ, given by Eq. (1), decreases with increasing temperature as the vibrational distribution, $\rho(u)$, broadens. The slope of $\langle u^2 \rangle$ vs. T ($\langle u^2 \rangle = k_B T/\phi$) therefore increases with increasing temperature as shown in Fig. 2(a). Thus using a simple model of anharmonic effects (e.g., the SCH model) and a simple potential (a Gaussian), a variation of $\langle u^2 \rangle$ with temperature

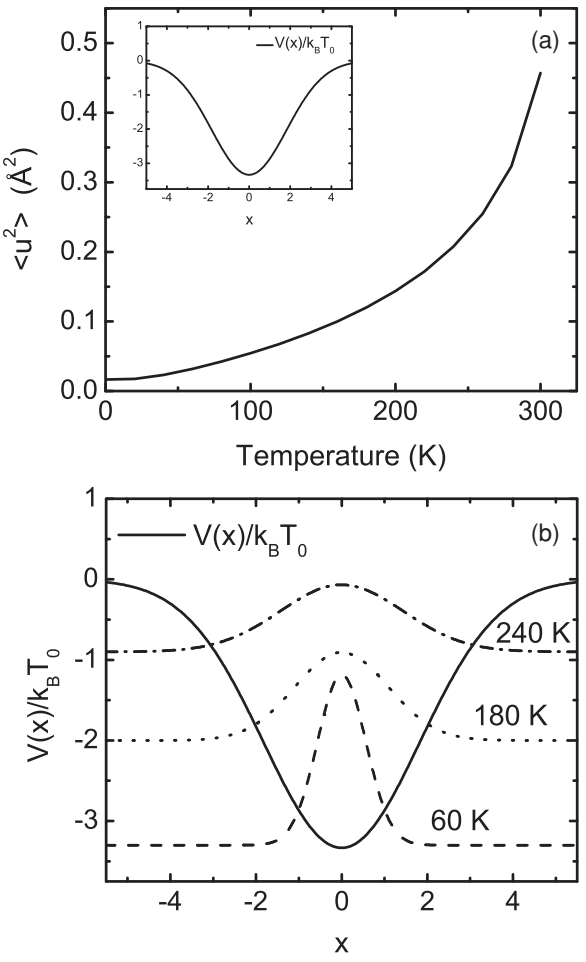

FIG. 2. (a) The MSD, $\langle u^2 \rangle$, of an atom in a Gaussian well, $V(x)$, where $x = u/u_0$. The slope of $\langle u^2 \rangle$ with temperature shows a marked increase at a $T \sim 250$ K simulating a dynamical transition at $T_D \sim 250$ K. (b) The vibrational distribution $\rho(x)$ in the Gaussian well at three temperatures.

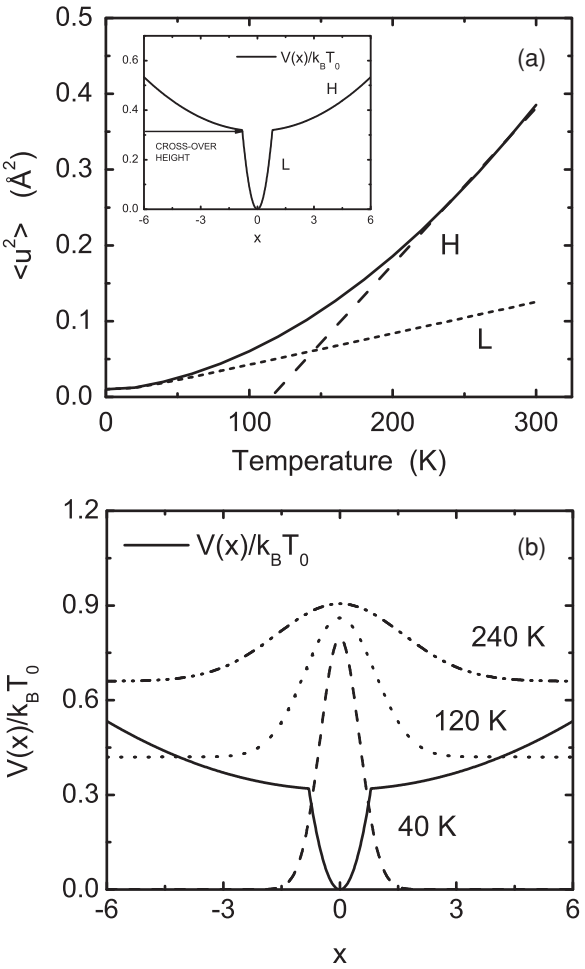

FIG. 3. (a) The $\langle u^2 \rangle$ in a potential well composed of two harmonic components characterized by force constants ϕ_L and ϕ_H. The slope crosses over gradually from a low (L) temperature to high (H) temperature value. (b) The $\rho(x)$ for a potential composed of two harmonic components.

as observed in biological macromolecules can be reproduced. The degree of change in slope of $\langle u^2 \rangle$ vs. T with increasing temperature depends entirely on the parameters chosen in the Gaussian potential. In the example shown in Fig. 2(b), the $\rho(x)$ begins to sample regions of $V(x)$ where d^2V/dx^2 is quite small (even negative) at a temperature of $T \simeq 250$ K. Thus the SCH force constant ϕ decreases rapidly with increasing T for $T \gtrsim 250$ K and the slope of $\langle u^2 \rangle = k_B T/\phi$ increases rapidly with increasing T for $T \gtrsim 250$ K.

Figure 3(a) shows the MSD $\langle u^2 \rangle$ for a particle in a potential that is the sum of two harmonic potentials as depicted in the inset of Fig. 3(a) and in Fig. 3(b). At low temperature, the slope of $\langle u^2 \rangle$ is set by the large force constant ϕ_L. This slope is indicated by the short dashed line in Fig. 3(a). At high temperature the slope of $\langle u^2 \rangle$ is set by the much smaller force constant ϕ_H that characterizes the shallow harmonic well at large values of x. The steeper slope of $\langle u^2 \rangle$ at higher temperatures is indicated by the long dashed line in Fig. 3(a). The temperature ($T \sim 150$ K) at which the slope crosses over from a low to a higher value depends on the energy at which the $V(x)$ crosses over from a large force constant ϕ_L to the smaller one, ϕ_H. The ϕ_H is adjustable. The crossover from the low (L) to high (H) temperature slope will always be gradual because the distribution $\rho(x)$ continues to sample the steep well potential near $x = 0$ at higher temperature, as shown in Fig. 3(b).

In Fig. 4 we show $\langle u^2 \rangle$ for a potential that is again the sum of two harmonic components but with a barrier between the two components. This potential leads to a $\langle u^2 \rangle$ which has the same basic character as that shown in Fig. 3(a). Thus introducing a barrier and displacing the minimum of the shallow potentials to finite values of x makes little difference to $\langle u^2 \rangle$. The $\langle u^2 \rangle$ in Figs. 3(a) and 4 are very similar probably because both potentials are symmetric about $x = 0$. The $\rho(x)$ are also similar and therefore the $\rho(x)$ for the potential depicted in Fig. 4 is not shown.

C. Asymmetric potentials

The four potentials $V(x)$ considered so far are symmetric around the origin ($x = 0$), i.e., symmetric around the center of the low-temperature well. This means that as temperature is increased, although $\langle x^2 \rangle$ increases, the vibrational distribution $\rho(x)$ remains centered around $x = 0$. We now consider

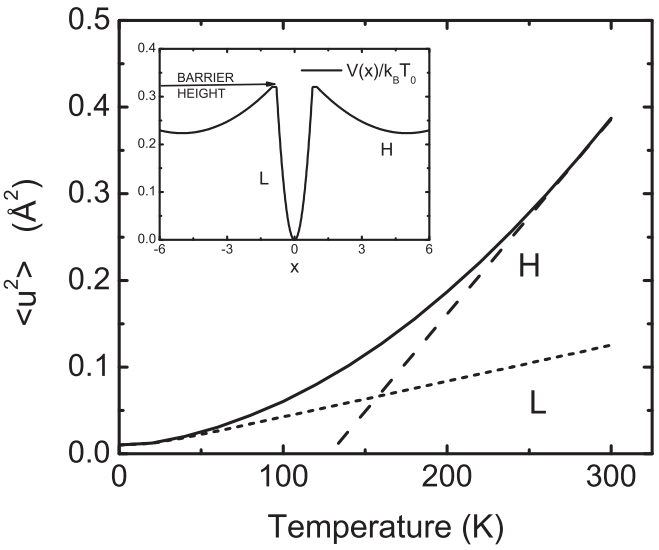

FIG. 4. The $\langle u^2 \rangle$ for an atom in a potential well composed of two harmonic components with a barrier separating the two components (see inset). The $\langle u^2 \rangle$ vs. temperature and $\rho(x)$ (not shown) is similar to that in Fig. 3(b).

potentials that are asymmetric around $x = 0$. This means that the center point of $\rho(x)$ will change with temperature. To accommodate this we generalize $\rho(x)$ to

$$\rho(x) = [2\pi \langle x^2 \rangle]^{-1/2} e^{-(x-\Delta)^2/2\langle x^2 \rangle}, \tag{6}$$

where as before $\langle x^2 \rangle = \langle u^2 \rangle / u_0^2$. The SCH $\langle x^2 \rangle$ and ϕ are obtained as before. The Δ is obtained by minimizing the potential energy $\langle V(x) \rangle$ as a function of Δ. Since we are in the classical limit, minimization of the free energy reduces to minimization of the potential energy.

Figure 5 shows the MSD for a particle in a double well potential. The double well potential selected consists of two harmonic wells (with force constant ϕ_L) separated by a barrier. At low temperature, the particle is confined to the left well ($x = 0$) with $\Delta = 0$, as indicated by the $\rho(x)$ in Fig. 5(b) for $T = 60$ K. As temperature is increased the center of the $\rho(x)$ moves to the right until at high temperature ($T = 240$ K) the $\rho(x)$ is centered symmetrically between the two wells. In the example shown in Fig. 5, the barrier height between the two wells is relatively small (compared to $k_B T_0$) and Δ moves from $\Delta = 0$ to the midpoint between the two wells at a relatively low temperature. This double well potential does not reproduce the observed increase in slope of $\langle u^2 \rangle$ with increasing temperature well.

In Fig. 6(a) we show the MSD for a particle in an asymmetric potential which is intended to simulate a particle near a surface or a wall. The wall on the LHS of the potential is formed by continuing the large low temperature force constant ϕ_L (near $x = 0$) to high energy ($\sim 2k_B T_0$). On the right-hand side (RHS), the "barrier height" of the low-temperature potential is low. Thus the particle can cross the barrier on the RHS and move to the right away from the wall at higher temperature. The potential on the RHS also has a well with a minimum or "well center" at $x \approx 3$. At higher temperature we anticipate that the particle will move toward the "well center." As shown in Fig. 6(a), the $\langle u^2 \rangle$ increases

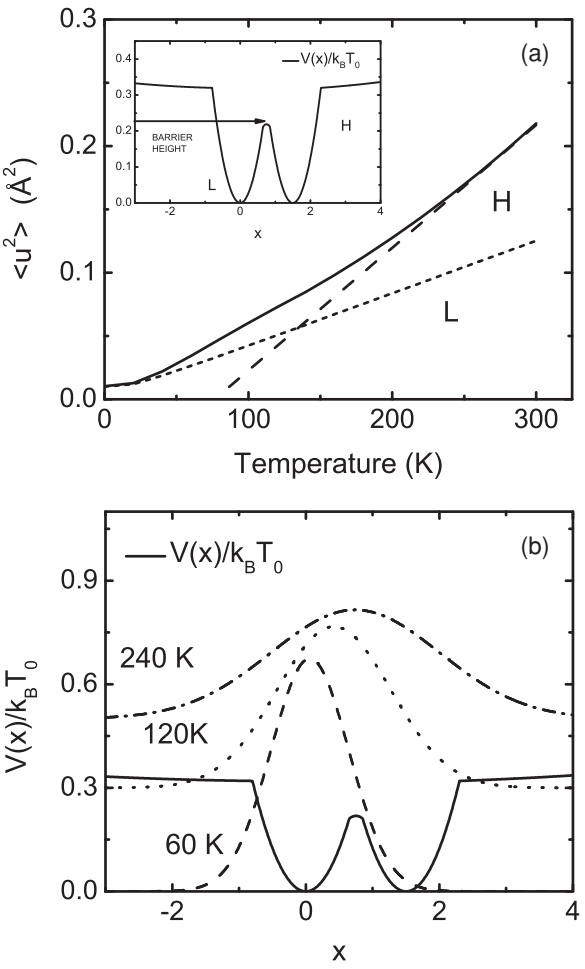

FIG. 5. (a) The MSD, $\langle u^2 \rangle$, for a double well potential. The height of the barrier (at $x_B = 0.75$) between the two wells (see inset) is relatively small, $V(x_B)/k_B T_0 \simeq 0.2$. (b) The $\rho(x)$ for a particle in a double well potential. The center of $\rho(x)$, Δ moves from one well ($\Delta = 0$) at $T = 0$ K to the midpoint between the two wells ($\Delta = x_B$) at a relatively low temperature. The slope at high temperature is set by the harmonic well force constant (H) at larger x.

very rapidly at high temperature ($T \sim 250$ K) with $\langle u^2 \rangle$ vs. T reaching a very steep slope at high temperature. The steep slope is associated with the particle moving rapidly away from the wall as T is increased, i.e., $\Delta(T)$ increasing rapidly with T at higher temperature.

The potential shown in Fig. 6 is a simple but very flexible potential which can reproduce a large or small change in slope of $\langle u^2 \rangle$ vs. T with the change in slope taking place at any desired temperature. It could also describe the eventual instability of a protein at an even higher temperature (as can the Gaussian potential). In Fig. 7 we show this potential with parameter (barrier height, well center, and ϕ_H) selected to reproduce the $\langle u^2 \rangle$ observed by Doster *et al.* [9] for hydrated myoglobin. Clearly, the change in slope seen in the data is well reproduced. In this potential, the slope at high temperature is set chiefly by the rate at which the particle is moving away from the wall (by the rate of change of $\Delta(T)$ with T) rather from the force constant ϕ_H describing the potential well on the RHS away wall. In this sense the physical origin of the slope

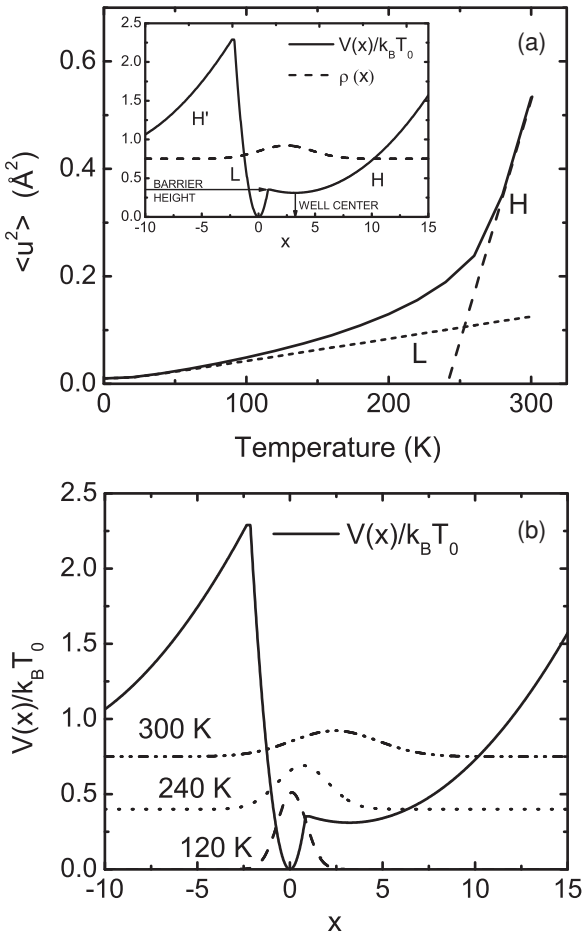

FIG. 6. (a) The MSD $\langle u^2 \rangle$ for a well that has a hard wall component. The $\langle u^2 \rangle$ vs. T shows a large increase in slope at $T \simeq 250$ K, an increase arising from the center of $\rho(x)$ moving rapidly away from the wall as T increases as shown in (b).

of $\langle u^2 \rangle$ at higher temperature is quite different from that for the symmetric Gaussian potential shown in Fig. 2.

IV. DISCUSSION

A. Dynamics of proteins

There are predominantly two approaches to revealing and understanding the dynamics of proteins. The first is experiment, chiefly neutron scattering experiments. The second is molecular dynamics (MD) simulation. The present work is neither of these. Rather it is an analytic approach using a simple model of the dynamics of an atom. The aim of the simple model is to make a single point, an important one we believe, that the change in slope of the observed $\langle u^2 \rangle$ versus T can be reproduced by a vibrating particle in an anharmonic potential. The model is simply anharmonic vibration with only temperature changing in the model. The present dynamical model does not contain any thermally activated, transition rate processes as in the "two-state" model introduced by Frauenfelder *et al*. [20], Keller and Debrunner [14], and Doster *et al*. [9]. It does not contain any diffusive motion.

In the classical limit, which is reached at $T \gtrsim 100$ K, the present MSD is independent of the mass of the particle. The

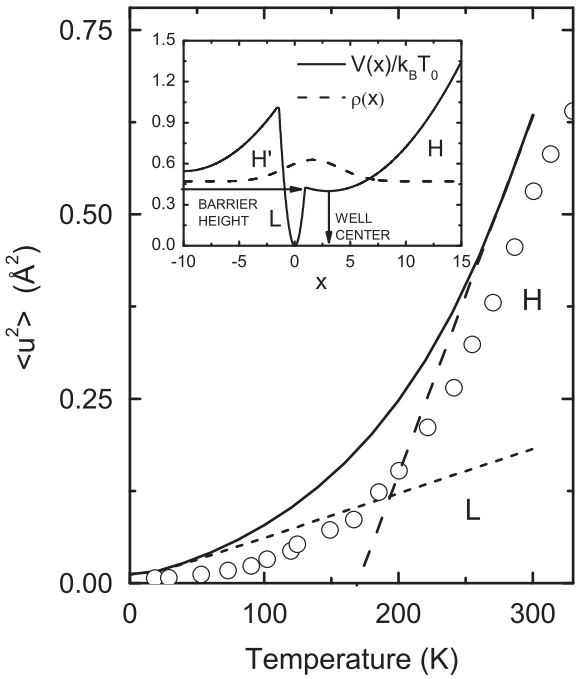

FIG. 7. The MSD $\langle u^2 \rangle$ for a well that has a hard wall component. The well parameters (ϕ_L, ϕ_H, barrier height, and well center) are adjusted to reproduce the $\langle u^2 \rangle$ vs. T observed for myoglobin by Doster *et al*. at low and high temperature. The observed values of Doster *et al*. [9] as presented in Ref. [4] are shown. The calculated $\langle u^2 \rangle$ clearly reproduce the observed $\langle u^2 \rangle$ for myoglobin well.

$\langle u^2 \rangle$ depends only on the potential, $V(u)$, selected and the temperature. The observed $\langle u^2 \rangle$ in proteins can be reproduced using a Gaussian potential or a potential with a wall. In the Gaussian potential, the slope of $\langle u^2 \rangle$ can change rapidly with temperature at a dynamical transition temperature T_D, if the second derivative of $V(u)$ changes rapidly with u at energies $V(u) \sim k_B T_D$. That is, if at energies $k_B T_D$, $V(u)$ becomes soft. A marked change in $\langle u^2 \rangle$ versus T will take place at T_D for any potential that has this property. For a potential with a wall, the slope of $\langle u^2 \rangle$ versus T changes at T_D because the particle moves away from the wall at $T \gtrsim T_D$. The slope is large for $T \geqslant T_D$ because the particle is moving rapidly away from the wall for $T \geqslant T_D$.

In the present model the change in slope of $\langle u^2 \rangle$ with T, with only T itself varying, is captured because the dynamical model is nonperturbative. That is, derivatives of $V(u)$ at displacements $u \geqslant 0$ [described here by $\rho(u)$] are sampled. A perturbative theory of anharmonic effects in which derivatives of $V(u)$ at $(u = 0)$ only are included would probably not suffice. Also since we are in the classical limit, the vibrational distribution $\rho(u)$ should be interpreted as representing a statistical distribution of the displacements of an ensemble of identical, independent classical particles in the well at temperature, T.

The model is adapted or adjusted to describe a specific protein by adjusting the low-temperature force constant ϕ_L in the model. We chose ϕ_L to reproduce the observed $\langle u^2 \rangle$ versus T of myoglobin at low temperature as observed by Doster *et al*. [9] (see also Fig. 1 of Bicout and Zaccai [4]) as depicted here in Fig. 1. Specifically, the parameters in the

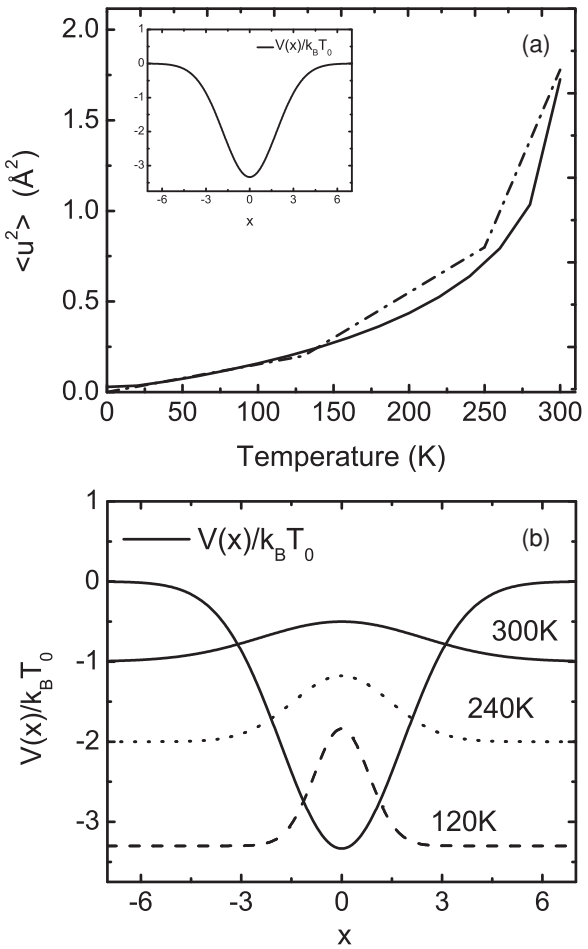

FIG. 8. (a) The calculated MSD $\langle u^2 \rangle$ for a Gaussian potential well (solid line). The low-temperature force constant ϕ_L of the Gaussian is set to reproduce the low temperature slope of $\langle u^2 \rangle$ vs. T in purple membrane (PM). The calculated $\langle u^2 \rangle$ at higher temperature for the Gaussian $V(u)$ reproduces the observed $\langle u^2 \rangle$ for PM (dashed-dotted line) well at higher temperature ($T \gtrsim 200$ K). The vibrational distribution $\rho(x)$ is shown in (b).

potential $V(u)$ are adjusted so that $[d^2V(u)/du^2]_{u=0} = \phi_L$. We can readily adjust the ϕ_L to reproduce other biological macromolecules such as purple membrane (PM) where at low temperature the slope of $\langle u^2 \rangle$ versus T is marginally larger [1]. This is shown in Fig. 8 for the Gaussian potential where we see that the observed $\langle u^2 \rangle$ versus T in PM is well reproduced at low and at high temperature using a Gaussian potential. Note that the definition of $\langle u^2 \rangle$ in Refs. [1] and [2] (Fig. 8) for PM is twice the value used in Refs. [9] and [14] (Fig. 7) for myoglobin.

MD and the SCP theory have been compared explicitly in solids. Specifically, the elastic constants [21], thermodynamic properties [22], and phonon response [23] in solids calculated using SCP theory at different levels of approximation and MD have been compared. For elastic constants, most appropriate here, the two agree accurately at intermediate temperatures but the SCP values can differ by up to 20% near the solid melting temperature where anharmonic effects are largest. At the same time MD simulations can show spurious dynamic response that is not found in SCP models or experiment. Thus we expect the SCP to be accurate up to intermediate temperatures and qualitatively correct but possibly 10–20 % in error at the highest temperatures.

B. Potentials in proteins

Neutrons scatter predominantly from hydrogen in proteins and interfacial water. In the following paragraphs we attempt a comparison of our model potentials with the potentials seen by hydrogen (H) in proteins. H in proteins is bound in a wide spectrum of sites and in solvent water. The H potential in these sites varies greatly. It depends on its separation from and on bond angles with its neighbors. The present simple model potentials represent an average over these widely varying potentials. To make a comparison we consider two simplified cases which represent two ends of the spectrum. We also ignore the dependence on angles. The first is hydrogen (H) in a hydrogen bond (H-bond) and the second is H in amino acids.

The dynamics of H in a H-bond is governed by the H-bond energy. As a simple example, we consider the H-bond in a single formamide dimer. The formamide dimer is, for example, a model bond used to represent H-bonds in protein backbones. The formamide dimer consists of a tightly bound N^- –H^+ pair which is hydrogen bonded to a second pair $O^- = C^+$, an acceptor-acceptor base pair. In the formamide dimer (N–H $\cdots$ $O = C$), the H-bond is the bond indicated by the dotted line between the H^+ (the donor H^+) and the acceptor O^- in the acceptor-acceptor base pair. Figure 9 shows the formamide H-bond energy versus separation r between the H and the acceptor (O), as calculated by Morozov and Kortemme [24] using density functional theory (DFT) (see Fig. 4 of Ref. [24]). The H-bond energy is divided by $k_B T_0 = 0.476$ kcal/mole $=$ 1.99 kJ/mole where $T_0 = 240$ K and the separation r by $u_0 = 0.33$ Å ($x = r/u_0$) so that the H-bond energy is in

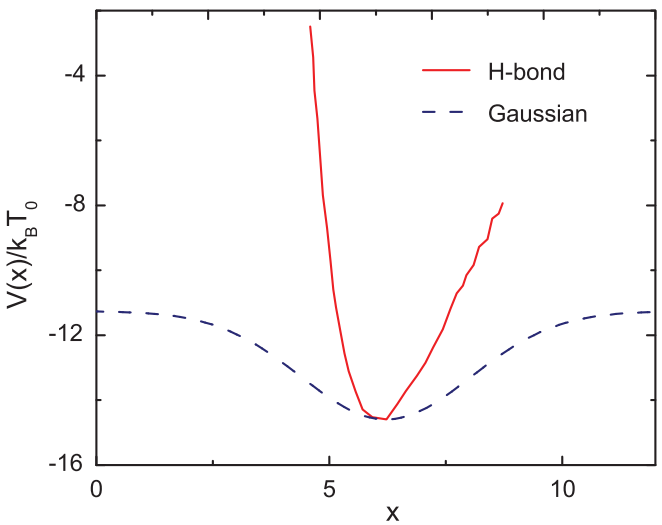

FIG. 9. (Color online) H-bond potential $V(r)$ in a formamide dimer versus H^+ to acceptor (O^-) separation, r, from Fig. 4 of Morozov and Kortemme [24]. The potential is shown in units $x = r/u_0$ where $u_0 = 0.33$ Å and $V(x)/k_B T_0$, where $T_0 = 240$ K and $k_B T_0 = 0.476$ kcal/mole. Also shown is the present Gaussian model potential in these units.

the same units as the present model potentials. The DFT energy is very similar to the H-bond energy obtained using molecular mechanics methods in which each atom in the bond interacts with a potential such as the CHARMM27 potential [25] or other potentials [27]. In the CHARMM27 potential, the interatomic potential is represented by a standard 12-6 Lennard-Jones potential [26] plus an electrostatic term [25]. In Fig. 9 the H-bond energy is compared with the present model Gaussian potential. The Gaussian well minimum is moved to coincide with that of the H-bond potential.

From Fig. 9 we see that the H-bond potential has clear anharmonic character as does the model present Gaussian potential. In addition the H-bond potential is asymmetric around the minimum energy. Both the anharmonic and asymmetric character will lead to an increase in slope of $\langle u^2 \rangle$ at higher temperature, as found here in Fig. 8 for the model Gaussian potential and in Fig. 6 for the model hard walled potential. As anticipated, the H-bond potential is much narrower and stronger than the model Gaussian. High-frequency, small amplitude motion is expected for H in a H-bond whereas the Gaussian represents an average for H over all sites.

Hydrogen is also attached to the backbone of proteins. In this position, the dynamics of the H is largely determined by the lower frequency, larger amplitude dynamics of the backbone. Specifically, H is a component of amino acids which make up the backbone and are attached to the backbone. To describe the dynamics of amino acids in the backbone, a simplified potential between amino acids is often introduced [28,29]. Each amino acid is approximated by a single (heavy) atom or pseudoatom. The effective or coarse-grained (CG) potential between the pseudoatoms is obtained using several methods one of which is simulating the amino acids in proteins using molecular dynamics (MD) and determining the effective interaction between them which best represents their properties. In the MD simulation a potential between all the atoms in the amino acids is typically used, denoted an all-atom potential. The CG potential is subsequently used to calculate the longer time scale dynamics of the backbone or of larger polypeptides in the protein The dynamics of H in these amino acids is largely governed by these CG potentials.

Specifically, Basdevant *et al.* [28] and Ha-Duong [30] represent the CG potential by a repulsive $(1/r^6)$ term plus a Gaussian attractive term. If the amino acid is charged there is also an electrostatic term. A representative CG potential between two TRP3 amino acids [28] is shown in Fig. 10 and compared with our model Gaussian potential. The CG potential is again shown with separation divided by $u_0 =$ 0.33 Å and energy divided by $k_B T_0$ so that it has the same units as our model potentials. The minimum of our Gaussian model potential has been shifted to coincide with that of the CG potential. From Fig. 10 we see that the CG potential is asymmetric and anharmonic so the a change is slope of $\langle u^2 \rangle$ with increasing temperature can be expected. Indeed the shape of the CG potential is similar to that of the the present hard wall potential as is shown in Fig. 11. The present hard wall model leads to a significant change of slope of $\langle u^2 \rangle$ with increasing temperature as shown in Fig. 7 and a similar change can be expected for the CG potential. From Fig. 10 we see that the CG potential is broader and weaker (on the right side) than

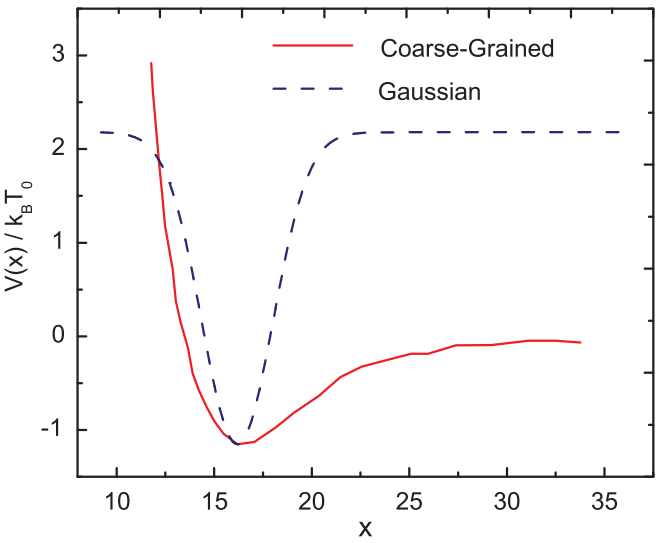

FIG. 10. (Color online) Coarse-grained potential $V(r)$ between two TRP3 amino acids in a protein from Fig. 3 of Basdevant *et al.* [28]. The potential is in units of $x = r/u_0$ and $V(x)/k_B T_0$ as in Fig. 9 and compared with the present Gaussian model potential.

our model Gaussian. Thus lower frequency, larger amplitude motions than average are expected for H in amino acids.

In summary, hydrogen in H-bonds and in amino acids see effective potentials that are anharmonic and similar in character to the model potentials used here. The H-bond potential is stiffer and the CG potential between amino acids is softer than the present model potentials which represent an average over a spectrum of potentials seen by H in proteins.

C. Concluding remarks

In summary, our aim in this paper is to illustrate that a change in slope of the MSD $\langle u^2 \rangle$ versus temperature can be obtained within vibration of a mass in an anharmonic potential. Our goal is not to say that thermally activated processes and

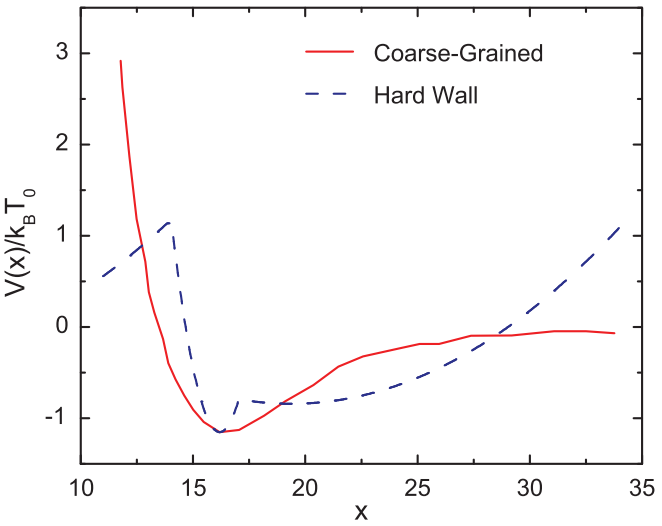

FIG. 11. (Color online) Coarse-grained potential shown in Fig. 10 compared with the present hard wall model potential.

diffusion are not important in the long time dynamics of proteins. The many dynamical processes that may contribute to the dynamical transition are reviewed by Doster [31]. Indeed, we have applied the present SCH vibrational dynamics to the "two-state" model potential introduced by Frauenfelder *et al*., Keller and Debrunner, and Doster *et al*. [9,14,20]. This potential coupled with the SCH dynamics did not lead to a $\langle u^2\rangle$ that agreed well with experiment—essentially because the thermally activated transitions central to this model are not included. Including the thermally activated transitions between the two states, as intended [9,14,20], is essential to obtain the good agreement with experiment that has been obtained using the "two state" model. Our purpose is simply to illustrate that a break in $\langle u^2\rangle$ with temperature is possible within vibration alone.

ACKNOWLEDGMENTS

It is a pleasure to thank Giuseppi Zaccai and Dominique Bicout for most helpful discussions and suggestions on this topic. Support from the US DOE under Grant No. DE-FG02-03ER46038 is gratefully acknowledged.

APPENDIX: THE SELF-CONSISTENT HARMONIC THEORY

In this section we derive the self-consistent harmonic theory for a single particle of mass M in an arbitrary potential $V(u)$, used in the present article. The particle is described by the Hamiltonian

$$\hat{H} = \hat{K} + V(u) \tag{A1}$$

where $\hat{K} = -(\hbar^2/2M)d^2/du^2$ is the kinetic energy operator. We introduce a model harmonic Hamiltonian

$$\hat{H}_h = \hat{K} + \tfrac{1}{2}\phi u^2 \tag{A2}$$

and corresponding harmonic density matrix

$$\rho_h = \frac{e^{-\beta H_h}}{Tr(e^{-\beta H_h})} \tag{A3}$$

where $\beta = (k_B T)^{-1}$. Expectation values evaluated using ρ_h are

$$\langle \hat{O}\rangle_h = Tr\{\rho_h \hat{O}\}, \tag{A4}$$

where $\hat{O}$ is any operator. The corresponding model harmonic Helmholtz free energy is

$$\begin{aligned} F_h &= \langle \hat{H}_h\rangle_h - TS_h \\ &= \langle \hat{H}_h\rangle_h + (k_B T)Tr\{\rho_h \log \rho_h\} \\ &= k_B T \log 2\sinh\left(\tfrac{1}{2}\beta\hbar\omega\right), \end{aligned} \tag{A5}$$

where $\omega = (\frac{\phi}{M})^{\frac{1}{2}}$ is the model simple harmonic oscillator frequency. In terms of $\hat{H}_h$ the particle $\hat{H}$ is

$$\hat{H} = \hat{H}_h + V(u) - \tfrac{1}{2}\phi u^2. \tag{A6}$$

The basic concept is to use ρ_h as a trial or model density matrix with which to evaluate the particle free energy. The trial particle free energy is

$$\begin{aligned} F_{\text{trial}} &= \langle H\rangle_h + (k_B T)Tr\{\rho_h \log \rho_h\} \\ &= F_h + \langle V(u)\rangle_h - \tfrac{1}{2}\phi\langle u^2\rangle_h. \end{aligned} \tag{A7}$$

The F_{trial} is an upper bound to the exact Helmholtz free energy, the Gibbs-Bogoliubov variational principle. We consider F_{trial} as a functional of the model harmonic force constant ϕ and the MSD $\langle u^2\rangle_h$. We minimize the F_{trial} with respect to ϕ and $\langle u^2\rangle_h$ independently holding the other variable constant to find the optimum ϕ and $\langle u^2\rangle_h$. This variation gives

$$\frac{\delta F_{\text{trial}}}{\delta\langle u^2\rangle_h} = \frac{1}{2}\left\langle \frac{d^2V(u)}{du^2}\right\rangle_h - \frac{1}{2}\phi = 0, \tag{A8}$$

$$\frac{\delta F_{\text{trial}}}{\delta\phi} = \frac{1}{2}\left(\frac{\hbar}{2M\omega}\right)\coth\left(\frac{1}{2}\beta\hbar\omega\right) - \frac{1}{2}\langle u^2\rangle_h = 0. \tag{A9}$$

The first term in Eq. (A8) is obtained by making a Taylor's expansion of $\langle V(u)\rangle_h$ in Eq. (A7) about $V(0)$, $V(u) = e^{u(\frac{d}{du})}V(0)$, and a cumulant expression of the exponential $\langle e^{u(\frac{d}{du})}\rangle_h$. For, a harmonic system with Gaussian distributions, $\langle u\rangle_h = 0$ and all cumulants beyond the second cumulant vanish so that

$$\begin{aligned} \langle V(u)\rangle_h &= \langle e^{u(d/du)}\rangle_h V(0) \\ &= e^{\frac{1}{2}\langle u^2\rangle_h (d^2/du^2)}V(0). \end{aligned} \tag{A10}$$

Differentiation with respect to $\langle u^2\rangle_h$ then yields the first term in Eq. (A8), and Eq. (A8) leads immediately to Eq. (A1) with $\langle\rangle_h$ expressed as a average in configuration space. The average in configuration space can be obtained by Fourier transforming $V(u)$ and again using a cumulant expansion,

$$\begin{aligned} \langle \nabla^2 V(u)\rangle_h &= \nabla^2 \int dq\, V(q)\langle e^{iqu}\rangle_h \\ &= \nabla^2 \int dq\, V(q) e^{-\frac{1}{2}q^2\langle u^2\rangle_h} \\ &= \int du e^{-\frac{1}{2}u^2/\langle u^2\rangle_h}\nabla^2 V(u), \end{aligned} \tag{A11}$$

where d/du is denoted by ∇. The first term in Eq. (A9) is obtained by differentiating Eq. (A5) for F_h with respect to ω using $\omega^2 = \phi/M$. Equation (A9) leads immediately to Eq. (3). The ϕ represents the optimum harmonic force constant representing a particle in an anharmonic well $V(u)$ in which the particle has a MSD $\langle u^2\rangle$.

[1] K. Wood, S. Grudinin, B. Kessler, M. Weik, M. Johnson, G. R. Kneller, D. Oesterhelt, and G. Zaccai, J. Mol. Biol. **380**, 581 (2008).

[2] K. Wood, U. Lehnert, B. Kessler, G. Zaccai, and D. Oesterhelt, Biophys. J. **95**, 194 (2008).

[3] S. Khodadadi, S. Pawlus, J. H. Roh, V. G. Sakai, E. Marnontov, and A. P. Sokolov, J. Chem. Phys. **128**, 195106 (2008).

[4] D. J. Bicout and G. Zaccai, Biophys. J. **80**, 1115 (2001).

[5] J. H. Roh, V. N. Novikov, R. B. Gregory, J. E. Curtis, Z. Chowdhuri, and A. P. Sokolov, Phys. Rev. Lett. **95**, 038101 (2005).
[6] J. H. Roh, R. M. Briber, A. Damjanovic, D. Thirumalai, S. A. Woodson, and A. P. Sokolov, Biophys. J. **96**, 2755 (2009).
[7] G. Zaccai, Science **288**, 1604 (2000).
[8] A. L. Tournier and J. C. Smith, Phys. Rev. Lett. **91**, 208106 (2003).
[9] W. Doster, S. Cusack, and W. Petry, Nature (London) **337**, 754 (1989).
[10] F. Parak, E. N. Frolov, A. A. Kononenko, R. L. Mossbauer, V. I. Goldanski, and A. B. Rubin, FEBS Lett. **117**, 368 (1980).
[11] B. Melchers, E. W. Knapp, L. Cordone, A. Cupane, and M. Leone, Biophys. J. **70**, 2092 (1996).
[12] A. P. Sokolov, H. Grimm, and R. Kahn, J. Chem. Phys. **110**, 7053 (1999).
[13] W. Doster, S. Cusack, and W. Petry, Phys. Rev. Lett. **65**, 1080 (1990).
[14] H. Keller and P. G. Debrunner, Phys. Rev. Lett. **45**, 68 (1980).
[15] S. H. Chen, L. Liu, E. Fratini, P. Baglioni, A. Faraone, and E. Mamontov, Proc. Natl. Acad. Sci. USA **103**, 9012 (2006).
[16] P. F. Choquard, *The Anharmonic Crystal* (W. A. Benjamin, New York, 1967).
[17] H. R. Glyde and M. L. Klein, Crit. Rev. Solid State Sci. **2**, 181 (1971).
[18] T. R. Koehler, Phys. Rev. Lett. **17**, 89 (1966).
[19] N. S. Gillis, N. R. Werthamer, and T. R. Koehler, Phys. Rev. **165**, 951 (1968).
[20] H. Frauenfelder, V. I. Goldanskii, and J. J. Hopfield (private communication to Keller and Debrunner).
[21] M. L. KLein and W. G. Hoover, Phys. Rev. B **4**, 537 (1971).
[22] M. L. KLein and W. G. Hoover, Phys. Rev. B **4**, 539 (1971).
[23] W. J. L. Buyers, G. Dolling, G. Jacucci, M. L. Klein, and H. R. Glyde, Phys. Rev. B **20**, 4859 (1979).
[24] A. V. Morozov and T. Kortemme, Adv. Protein Chem. **72**, 1 (2005).
[25] A. D. MacKerrell *et al*., J. Phys. Chem. B **102**, 3586 (1998).
[26] J. E. Lennard-Jones, Proc. R. Soc. London A **106**, 463 (1924).
[27] C.-L. Sun and C.-S. Wang, J. Mol. Struct., Theochem **956**, 38 (2010).
[28] N. Basdevant, D. Borgis, and T. Ha-Duong, J. Chem. B **111**, 9390 (2007).
[29] M. R. Betancourt and S. J. Omovie, J. Chem. Phys. **130**, 195103 (2009).
[30] T. Ha-Duong, J. Chem. Theory Comput. **6**, 761 (2010).
[31] W. Doster, BBA Proteins and Proteomics **1804**, 3 (2010).